Theoretical Study of SOA-Based Wavelength Conversion with NRZ and RZ Format at 40 Gb/s *

DONG Jian-Ji(董建绩)[1], ZHANG Xin-Liang(张新亮)[1**], FU Song-Nian(付松年)[2], SHUM Ping(沈平)[2], HUANG De-Xiu(黄德修)[1]

[1] *Wuhan National Laboratory for Optoelectronics, Huazhong University of Science and Technology, Wuhan 430074*
[2] *Network Technology Research Centre, Nanyang Technological University, Singapore 637553*

(Received 8 December 2006)

We theoretically discuss 40 Gb/s semiconductor optical amplifier (SOA)-based wavelength conversion (WC) using a detuning optical bandpass filter based on ultrafast dynamic characteristics of SOA. Both the inverted and non-inverted WCs are obtained by shifting the filter central wavelength with respect to the probe wavelength when input data signal is in return-to-zero (RZ) format. However, we can obtain format conversion from nonreturn-to-zero (NRZ) to pseudo-return-to-zero (PRZ) and inverted WC when the input signal is in NRZ format.

PACS: 42. 79. Nv, 85. 60. − q

All-optical wavelength conversion (WC) based on semiconductor optical amplifiers (SOAs) has received considerable attention during the past years because of small footprint, low power consumption, and optical integration.[1−3] However, the relatively slow gain recovery time of SOAs (typically about 100 ps) limits the maximum operation speed. Currently the all-optical signal processing technique based on transient cross-phase modulation (T-XPM) of SOAs is a promising technique, which not only provides high speed operation, but also has the advantage of simple configuration.[4] The structure of T-XPM consists of an SOA and a detuning optical bandpass filter (OBF). The key point is that the injected data signal should be ultrashort pulses (< 10 ps), and the consequent OBF has some detuning to the probe signal. Nielsen *et al.*[5] presented a 40 Gb/s non-inverted WC by employing an OBF to select the blue-shifted part of the probe spectrum. Liu *et al.*[6] presented the 320 Gb/s inverted WC by selecting the blue-shifted probe spectrum. Besides the high speed WC, the T-XPM technique has been applied to optical demultiplexing,[7] optical logic gates,[8] and optical adders,[9] etc.

In this Letter, we theoretically study the multifunctional WC at 40 Gb/s based on the T-XPM technique. Both inverted and non-inverted WCs at 40 Gb/s are simulated with blue-shifted OBF when the input signal is in return-to-zero (RZ) format. These simulations are in good agreement with our recent experimental data.[10] When the input signal is nonreturn-to-zero (NRZ) format, simulations show both format conversion from NRZ to pseudo-return-to-zero (PRZ) and inverted WC with different OBF detunings.

The multifunctional WC based on T-XPM is schematically illustrated in Fig. 1. A cw probe beam at wavelength λ_c is combined with another modulated data signal with the RZ format or NRZ format and launched into the SOA. The data signal will modulate the phase and gain of probe beam at a different wavelength through the carrier dynamics. The subsequent OBF has some detuning to the probe signal with the central wavelength $\lambda_c + \Delta\lambda_{\rm det}$, where $\Delta\lambda_{\rm det}$ is the detuning value from probe wavelength λ_c. It is noticed that the positive/negative value of $\Delta\lambda_{\rm det}$ should be considered as the OBF red-shifted/blue-shifted.

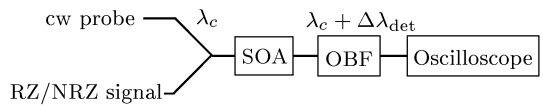

Fig. 1. Illustration of multifunctional WC based on T-XPM.

In order to explore the intrinsic mechanism of our proposed scheme, a potent SOA model should be developed to predict the SOA operation. The theory of Agrawal and Olsson assumes that the gain saturation of the SOA is caused only by the depletion of carrier density owing to stimulated emission and neglects the main intraband processes, such as spectrum hole burning (SHB) and carrier heating (CH).[11] However, when the SOA is operated with pulses shorter than a few picoseconds, intraband effects become more important. The theory of Mecozzi and Mørk is a simple and powerful method for calculating the amplification of picosecond pulses in an SOA.[12] Therefore we amend our previous model[13] with their theory associ-

* Supported by the National High Technology Developing Programme of China under Grant No 2006AA03Z0414, the National Natural Science Foundation of China under Grant No 60407001, and the New Century Excellent Talent Project in the Ministry of Education of China under Grant No NCET-04-0715.

** Email: xlzhang@mail.hust.edu.cn

©2007 Chinese Physical Society and IOP Publishing Ltd

ated with the intraband mechanism. Then the material gain can be expressed as $\bar{g} = g_l/(1+\varepsilon P_{\rm tot})$, where $P_{\rm tot}$ is the total input power coupled into the SOA, ε is the nonlinear gain suppression factor associated with the SHB and CH effects, $\varepsilon = \varepsilon_{\rm CH} + \varepsilon_{\rm SHB}$, and g_l is the linear material gain coefficient described in Ref. [13] in detail. Then we combine this SOA model with a typical Gauss filter model to simulate the proposed multifunctional WC. More detailed description has been presented in Ref. [14]. No matter whether the input data signal is RZ format or NRZ format, our model is expected to be reasonably accurate.

Now we discuss the WC of RZ signal with ps-scale pulses. When the 2.5 ps-wide RZ signal is injected into an SOA with $\varepsilon = 0.6$, the phase shift $\Delta\Phi$ and chirps $\Delta\nu$ of the probe signal are plotted in Fig. 2. We notice that in Fig. 2(a), $\Delta\Phi$ is divided into two parts, $\Delta\Phi_N$ due to carrier density modulation and $\Delta\Phi_{\rm CH}$ due to CH contribution, which respond to the slow recovery and fast recovery of converted signal, respectively. Figure 2(b) shows the chirp variations, where the red peak and blue peak are related to the slope of the leading edge and trailing edge of the phase.

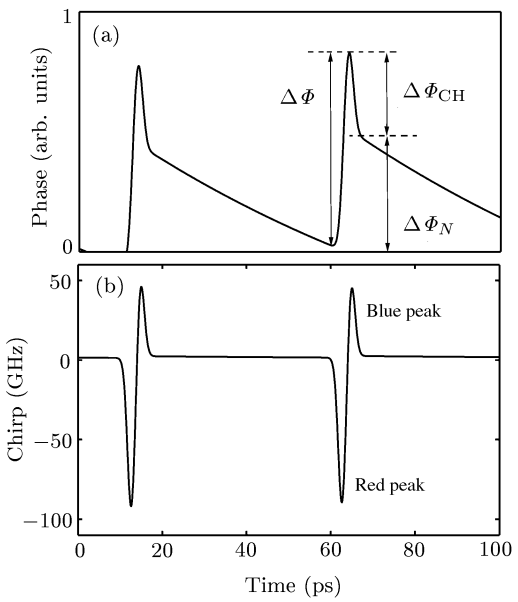

Fig. 2. (a) The temporal phase variation and (b) the temporal chirp variation.

When the input RZ signal is 8-bit stream 11110010 with 2.5 ps pulsewidth modulated at 40 Gb/s, we simulate the normalized power distribution of the converted signal in the time domain when the OBF detuning varies from -0.8 nm to 0.8 nm, as shown in Fig. 3(a). We find several special power distribution lines corresponding to $\Delta\lambda_{\rm det} = 0.8$ nm, -0.8 nm, 0 nm and -0.32 nm. The crosses are the extremal points where the power is either zero or one. When $\Delta\lambda_{\rm det} = 0.8$ nm and -0.8 nm, we plot the converted waveforms in Fig. 3(b). In such a case, it functions as a non-inverted WC, except that some pattern effects occur. The pattern effect here is named as nonlinear patterning (NLP), which results from carrier density saturation. When $\Delta\lambda_{\rm det} = 0$ nm and -0.32 nm, we plot the converted waveforms in Fig. 3(c). In such a case, it functions as inverted WC; however, the converted waveform of $\Delta\lambda_{\rm det} = -0.32$ nm has much higher extinction ratio (ER) and much weaker pattern effects than that of $\Delta\lambda_{\rm det} = 0$ nm. This reveals that a blue-shifted OBF can accelerate gain recovery of inverted WC and can reduce the pattern effect.

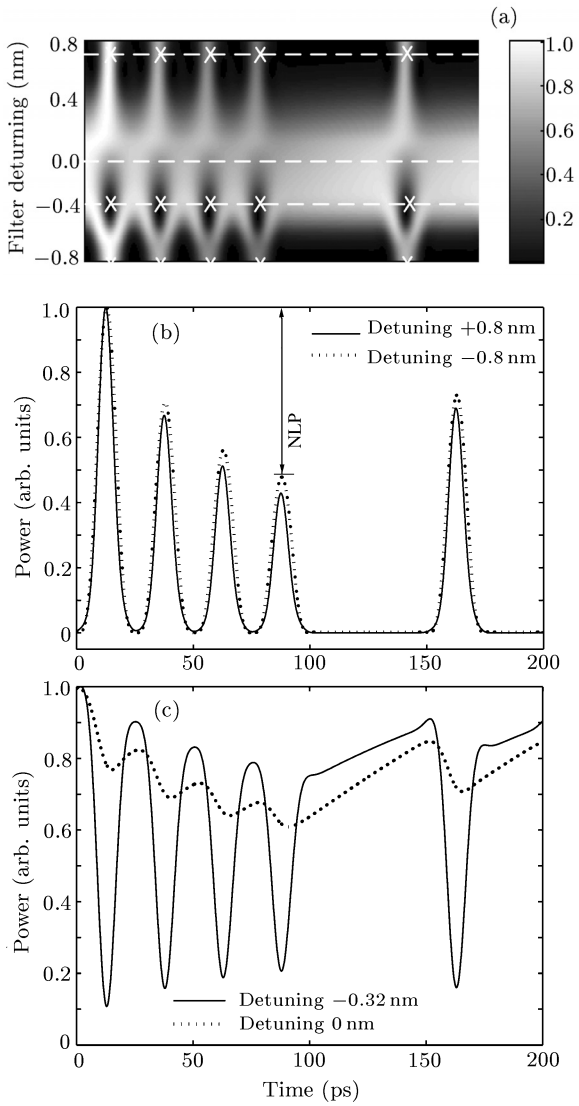

Fig. 3. Output waveforms with different detunings: (a) the normalized power distribution with different detunings, (b) non-inverted WC when the detuning is 0.8 nm and -0.8 nm, (c) inverted WC when the detuning is -0.32 nm and 0 nm.

It is interesting that the non-inverted WC can be obtained by large OBF detuning (either blue- or red-shifted), while the inverted WC can be obtained by

small OBF detuning (blue-shifted). This can be explained as follows. The input RZ signal will induce transient nonlinear phase shifts and intensity modulation to the probe signal via cross-phase modulation (XPM) and cross-gain modulation (XGM) in the SOA. The nonlinear phase shifts will result in a chirped converted signal with the broadened spectrum. On the one hand, the chirped probe wavelength shift occurs only in the leading edges or the trailing edges of input RZ signal. When the OBF is detuned far away from the probe wavelength to select such probe energy at shifted components and to suppress the probe carrier, the mark of output waveforms appears in the leading edges or trailing edges of input RZ signal, and the space appears in another timeslot. As a result, the converted signal will keep in-phase to the input RZ signal. This is non-inverted WC. On the other hand, the XGM will result in the inverted WC with relatively slow recovery if there is no filter detuning, whereas the blue-shifted OBF can balance the power of blue chirped component and the probe power during gain recovery. The power is increasing during the gain recovery while the power of blue chirped component is decreasing. As a result, the net power at the filter output is approximately constant. This means that the system effectively recovers much faster than the SOA gain. In addition, the blue-shifted filter will make the gain pit much lower, therefore the ER will be improved compared with no detuning. These simulation results are validated by our recent experimental report.[10]

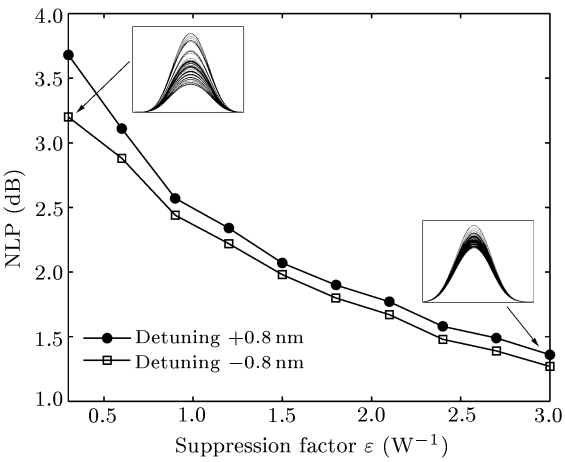

Fig. 4. NLP variation with respect to the gain suppression factor when the detuning is 0.8 nm and −0.8 nm.

The NLP, resulting from gain saturation, cannot be easily suppressed. Here we discuss the gain suppression factor and input pulsewidth on the NLP. Figure 4 shows the NLP variation with respect to ε when the detuning is 0.8 nm and −0.8 nm. Gain suppression factor ε is an important parameter, which denotes the strength of intraband effects. The NLP will decrease as ε increases. This is because the strong intraband effects can deepen the SOA gain modulation, then the NLP can be reduced.

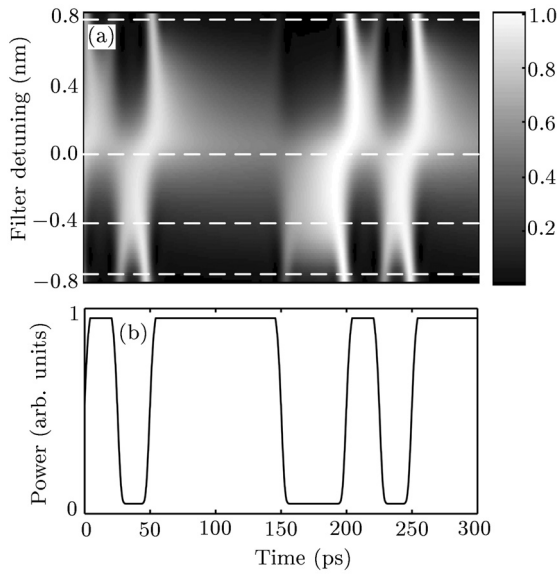

Fig. 5. (a) Normalized power distribution with different detunings, (b) input NRZ waveform.

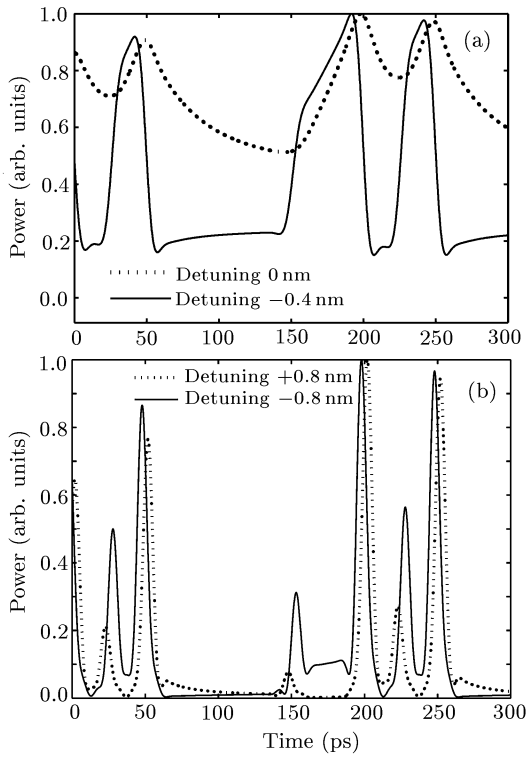

Fig. 6. Output waveform with different detunings: (a) inverted WC when the detuning is 0 nm and −0.4 nm, (b) format conversion from NRZ to PRZ when the detuning is −0.8 nm and 0.8 nm.

Now we discuss the 40 Gb/s WC with NRZ for-

mat. Based on the SOA model mentioned above, we simulate the normalized power distribution of the converted signal in the time domain when the OBF detuning varies from -0.8 nm to 0.8 nm, as shown in Fig. 5(a). In the simulation, the input NRZ waveform at 40 Gb/s is shown in Fig. 5(b). From Fig. 5(a), good inverted WC can be confirmed in the blue-shifted region, e.g. at detuning of -0.4 nm. Then we plot the output waveforms when the detuning is -0.4 nm and 0 nm in Fig. 6(a). This shows that the blue-shifted OBF can accelerate the recovery with NRZ format WC and can improve the output ER, compared to the case of non-detuning. This can be explained in a similar way to the RZ format case. When the detuning is very large, such as 0.8 nm or -0.8 nm, we find that the peaks of output power appear at the leading edges or trailing edges of the input NRZ signal. We plot the converted waveforms in Fig. 6(b). In such a case, it completes the format conversion from NRZ to PRZ. The phase shift of converted signal occurs only in the leading edges or the trailing edges of input NRZ signal, so a large detuning OBF could convert the phase information to intensity information. Although the PRZ signal has nonuniform amplitude, it is very useful to complete clock extraction since it contains the clock components.

In summary, we have proposed and demonstrated theoretically the multifunctional WC at 40 Gb/s using a single SOA followed by a detuning filter. When the input signal is RZ format, we obtain both inverted and non-inverted WCs by different detunings of the filter. When the input signal is in NRZ format, we obtain both inverted WC and format conversion to PRZ with different detunings of the filter.

References

[1] Chow K K, Shu C, Mak M W K and Tsang H K 2002 *IEEE Photon. Technol. Lett.* **14** 1445

[2] Xu F, Zhang X L, Liu H R, Liu D M and Huang D X 2006 *Chin. Phys. Lett.* **23** 355

[3] Chen G X, Li W, Huang W P and Jian S S 2005 *Chin. Phys. Lett.* **22** 110

[4] Nakamura S and Tajima K 1997 *Appl. Phys. Lett.* **70** 3498

[5] Nielsen M L, Lavigne B and Dagens B 2003 *Electron. Lett.* **39** 1334

[6] Liu Y, Tangdiongga E, Li Z, deWaardt H and Koonen A M J 2006 *OFC/NFOEC* paper PDP28

[7] Tangdiongga E, Liu Y, deWaardt H, Khoe G D and Dorren H J S 2006 *IEEE Photon. Technol. Lett.* **18** 908

[8] Li Z, Liu Y, Zhang S, Ju H, de Waardt H, Khoe G D, Dorren H J S and Lenstra D 2005 *Electron. Lett.* **41** 1397

[9] Dong J, Fu S, Zhang X, Shum P, Xu J and Huang D 2007 *Opt. Commun.* **270** 238

[10] Dong J, Zhang X, Xu J, Huang D, Fu S, Shum P and Gong Y 2007 *OFC/NFOEC* (USA March 2007)

[11] Agrawal G P and Olsson N A 1989 *IEEE J. Quantum Electron.* **25** 2297

[12] Mecozzi A and Mork J 1997 *IEEE J. Select. Top. Quantum Electron.* **3** 1190

[13] Dong J, Zhang X, Jiang Z and Huang D 2005 *Opt. Quantum Electron.* **37** 1011

[14] Dong J, Zhang X, Xu J, Huang D, Fu S and Shum P 2007 *Opt. Exp.* (accepted)